

Interdecadal Modulation of mega-ENSO on the North Pacific Atmospheric Circulation in Winter

Journal:	<i>Atmosphere-Ocean</i>
Manuscript ID	AO-2016-0021
Manuscript Type:	Fundamental Research / Recherche fondamentale
Date Submitted by the Author:	21-Jun-2016
Complete List of Authors:	Zhang, Peng; Nanjing University of Information Science and Technology Wu, Zhiwei; Nanjing University of Information Science & Technology, School of Atmospheric Sciences Chen, Hua; Nanjing University of Information Science and Technology
Keywords:	Climate Change < atmosphere and hydrology, Climate Variability < atmosphere and hydrology, Pacific < location, Observational < type of work, Modeling < type of work

SCHOLARONE™
Manuscripts

1
2
3
4 1 **Interdecadal Modulation of mega-ENSO on the North**
5
6 2 **Pacific Atmospheric Circulation in Winter**
7
8 3

9 4 Peng Zhang, Zhiwei Wu and Hua Chen
10 5

11 6 *Earth System Modeling Center, Nanjing University of Information Science*
12 7 *&Technology, Nanjing, Jiangsu 210044, China*
13 8
14 9
15 10
16 11
17 12
18 13
19 14
20 15
21 16
22 17
23 18
24 19
25 20
26 21
27 22
28 23
29 24
30 25
31 26
32 27
33 28
34 29
35 30
36 31
37 32
38 33
39 34
40 35
41 36
42 37
43 38
44 39
45 40
46
47
48
49
50
51
52
53
54
55
56
57
58
59
60

June 21, 2016

Submitted to *Atmosphere-Ocean*

34 **Corresponding author:**

35 Prof. Zhiwei Wu

36 Earth System Modeling Center, Nanjing University of Information Science &
37 Technology, Nanjing, Jiangsu 210044, China

38 Email: zhiweiwu@nuist.edu.cn
39
40

Abstract

The mega-El Niño/Southern Oscillation (ENSO) is a principal component of the global air-sea coupling system. Its impact on the atmospheric circulation over the North Pacific is crucial for decadal climate predictions in the Northern Hemisphere. Observational analysis in this study indicates that the mega-ENSO has experienced a notable inter-decadal change in its connection with the winter West Pacific teleconnection pattern (WP) and the Aleutian Low during the past 56 years. It is significantly correlated with the WP during 1957–1975, yet such an intimate linkage breaks down and is replaced by the Aleutian Low after 1979. Numerical evidences show that such apparent change might be attributed to the change of sea surface temperature anomaly (SSTA) over the extra-tropical North Pacific (XNP). The WP pattern is excited in the upper troposphere when there is a mega-ENSO-like SSTA without the XNP SSTA, whereas an Aleutian Low type response is concurrent with the mega-ENSO and XNP SSTAs. Two factors might be related to the generation of the XNP SSTA. One is the mega-ENSO itself, and the other is the extra-tropical North Atlantic SSTA. The potential physical mechanisms are also discussed.

58 1. Introduction

59 The mega-El Niño/Southern Oscillation (ENSO) is an integrated feature of the
60 interannual-to-interdecadal variation of global sea surface temperature (SST), and
61 reflects a broader range of variability than ENSO, the Pacific Decadal Oscillation
62 (PDO) and the Interdecadal Pacific Oscillation (IPO) alone (Wang et al., 2013). We
63 have known that the dynamic mechanism of PDO could be recognized as a
64 phenomenon of the tropical (Cane et al., 1995; Yukimoto et al., 1996) and
65 mid-latitude (Latif et al., 1994, 1996) air-sea interactions as well as their coupled
66 effects (Gu and Philander, 1997). ENSO could be explained by tropical air-sea
67 interactions, relaxation of the trade winds or other theories (Bjerknes, 1966; Wytki,
68 1975; Philander, 1981; and others). The mega-ENSO was related to an off-equatorial
69 atmosphere-ocean thermodynamic feedback between the two Pacific subtropical highs
70 (PSHs)/trades and basin-wide SST anomalies (SSTAs) (Wang et al., 2015). With a
71 much broader spatial-temporal scale, the mega-ENSO is likely to exert more profound
72 influences on global climate than a conventional ENSO. Up to now, there have been
73 many studies on ENSO and its climate impacts (Charney and Shukla, 1981;
74 Ropelewski and Halpert, 1986; Jin et al., 1994; Zhang et al., 1996; Neelin et al., 1998;
75 Chang et al., 2000; Wang et al., 2000, 2008; Wu and Li, 2008, 2009; Wu et al., 2009;
76 Wu and Lin, 2012; and many others), but few on the mega-ENSO (Wu and Zhang,
77 2014; Wu and Yu, 2015; Wang et al., 2015; Kim and Ha, 2015). This motivates the
78 current study.

79 The climate variability in the North Pacific has drawn considerable attentions in

1
2
3
4 80 recent years because of its impact on both tropical and extra-tropical climate (Hsu and
5
6 81 Wallace, 1985; Deser et al., 1999; Graham, 1994; Latif and Barnett, 1994, 1996;
7
8 82 Barlow et al., 2001; Ceballos et al., 2009; He et al., 2013b; Oshika et al., 2014). There
9
10
11 83 are two dominant modes of atmospheric variability over the North Pacific. One is
12
13
14 84 linked to the changes of the Aleutian Low and its temporal evolution can be quantified
15
16 85 by the North Pacific index (NPI) (Trenberth and Hurrell, 1994). The other is the North
17
18 86 Pacific Oscillation (NPO) (Walker and Bliss, 1932; Rogers, 1981), with the
19
20
21 87 upper-tropospheric geopotential height showing the West Pacific (WP) teleconnection
22
23
24 88 pattern (Wallace and Gutzler, 1981; Linkin and Nigam, 2008). The winter variability
25
26 89 of the Aleutian Low is associated with the Pacific/North American (PNA) as well as
27
28
29 90 the variability of the Arctic as Arctic Oscillation (AO) (Overland, 1999), and its
30
31 91 influence in the Northern Hemisphere is evident from the surface (Maslanik et al.,
32
33
34 92 1996) to the stratosphere (Kodera et al., 1996). In comparison with the PNA and
35
36 93 North Atlantic Oscillation (NAO), the WP pattern has received relatively little
37
38
39 94 attention, although it exerts a profound influence on winter continental precipitation in
40
41 95 the Northern Hemisphere (Nigam, 2003; Linkin and Nigam, 2008). The negative WP
42
43
44 96 phase can also affect the Eastern Asian monsoon and lead to abnormally cool
45
46 97 temperatures over Eastern Eurasia in the winter (Gong et al., 2001; Zhang et al.,
47
48
49 98 2009).

50
51 99 The association of atmospheric circulation over the North Pacific with ENSO
52
53
54 100 has also been widely examined. From previous studies, it is known that the boreal
55
56 101 winter near-surface atmospheric circulations over the North and Central Pacific
57
58
59
60

1
2
3
4 102 influence the state of the tropical Pacific and can initiate the development of ENSO
5
6 103 events (Anderson et al., 2013; Anderson and Renelley, 2015). Conversely, circulations
7
8
9 104 over the North Pacific are also affected by tropical SSTA-. Bjerknes (1966, 1969) first
10
11 105 noted that the Aleutian Low tends to strengthen and shift southeastward during El
12
13
14 106 Niño events. Trenberth and Hurrell (1994) found that the deepened Aleutian Low in
15
16
17 107 ENSO events results in a unique SSTA pattern that, on average, is enhanced through
18
19 108 the effects of the extratropical SSTA itself. Meanwhile, ENSO is also a well-known
20
21 109 key factor for long-term prediction of the WP pattern (Horel and Wallace, 1981; Mo
22
23
24 110 and Livezey, 1986; Kodera, 1998; Oshika et al., 2014). Horel and Wallace (1981)
25
26
27 111 showed that winter El Niño events are usually associated with the positive phases of
28
29 112 the winter WP. As a matter of fact, considerable evidences have emerged of a
30
31 113 decade-long change since the mid-1970s in the North Pacific atmosphere and ocean
32
33
34 114 (Trenberth, 1990; Trenberth and Hurrell, 1994; Hanawa et al., 1996; Overland, 1999).
35
36
37 115 The oceanic change is characterized by a cooling SSTA in the central and western
38
39 116 North Pacific and a warming SSTA in the eastern tropical Pacific since 1976
40
41
42 117 (Trenberth, 1990; Deser et al., 1996; Guilderson and Schrag, 1998). The atmospheric
43
44
45 118 change includes an intensification and eastward shift of the Aleutian Low (Trenberth,
46
47 119 1990; Graham, 1994; Trenberth and Hurrell, 1994). Such interdecadal changes of the
48
49 120 ocean-atmosphere system could strongly affect and modulate the interannual
50
51
52 121 relationship between the tropical SSTAs and the atmospheric circulation and further
53
54 122 affect regional climate such as the East Asian Winter Monsoon (Ding et al., 2010; He
55
56
57 123 and Wang, 2013a).

1
2
3
4 124 In contrast to ENSO and PDO, the mega-ENSO has its own characteristics.
5
6 125 Wang et al. (2013) first revealed that mega-ENSO contributed to the intensification
7
8 126 of the Northern Hemisphere summer monsoon during the past decades, which was
9
10 127 not obvious in the conventional ENSO. Wu and Yu (2015) found that dynamic
11
12 128 models would exhibit a high skill in the East Asian Summer Monsoon (EASM)
13
14 129 hindcast if the relationship between the EASM and mega-ENSO was captured. Kim
15
16 130 and Ha (2015) revealed that the mega-ENSO index was better than the PDO index
17
18 131 for denoting tropical Pacific characteristics, because the mega-ENSO index could
19
20 132 well capture the easterly moisture transport over the tropics, but the PDO index
21
22 133 could not. Wu and Zhang (2014) pointed out that the mega-ENSO experiences a
23
24 134 notable inter-decadal change in its linkage with the winter NAO during the past 56
25
26 135 years, and this marked change might be attributed to the SST forcing change in the
27
28 136 North Atlantic. Up to now, understanding the origin of the interdecadal variability in
29
30 137 the northern hemisphere (particularly the mid-high latitudes) is a challenging issue.
31
32 138 And it remains an open question whether the mega-ENSO can modulate the North
33
34 139 Pacific atmospheric circulation. If so, what is the physical mechanism responsible for
35
36 140 it? This work attempts to answer the above questions.
37
38
39
40
41
42
43
44
45

46 141 The current paper is structured as follows. Section 2 describes the data, model
47
48 142 and experimental design. The distinctive mega-ENSO-related atmospheric
49
50 143 circulation anomalies between 1957–1975 and 1979–2012 are examined in Section 3.
51
52 144 Section 4 compares the differences of the three-dimensional circulation structures
53
54 145 associated with mega-ENSO during these two epochs. In Section 5, the modulating
55
56
57
58
59
60

1
2
3
4 146 effect of the extra-tropical North Pacific (XNP) SSTA is discussed, and an
5
6 147 atmospheric general circulation model (AGCM) and coupled general circulation
7
8 148 model (CGCM) are utilized to assess the mechanisms. The last section summarizes
9
10
11 149 the paper.
12
13
14
15

151 **2. Data, model and experiments**

152 The data used in this study include: (1) monthly mean Japanese 55-year
153 Reanalysis data (JRA-55) (Kobayashi et al., 2015) from 1958 to 2013; (2) monthly
154 mean SST data of the Hadley Centre sea ice and sea surface temperature (HadISST)
155 (Rayner et al., 2003).
156

157 The mega-ENSO index is defined in this study as the SST difference between
158 the western Pacific K-shape area and eastern Pacific triangle area, as shown in figure
159 3 in Wang et al. (2013). In order to be consistent with other ENSO indices, the sign
160 of the mega-ENSO index has been reversed. The definition of the WP index follows
161 the description of Wallace and Gutzler (1981) and Barnston and Livezey (1987),
162 which is the 500-hPa geopotential height (Z500) difference between (60°N, 155°E)
163 and (30°N, 155°E). The NP index is defined as the area-weighted sea level pressure
164 over the region of (30°N–65°N, 160°E–140°W), and is used to characterize the
165 temporal evolution of the Aleutian Low (Trenberth and Hurrell, 1994). These two
166 indices were taken from the NOAA/Earth System Research Laboratory (ESRL)
167 (online at <http://www.esrl.noaa.gov/psd/data/climateindices/list/>). The spatial pattern
of the Aleutian Low and the WP teleconnection at 500-hPa are shown in Figure 1.

1
2
3
4 168 The PDO index used in this study is constructed according to the definition given by
5
6 169 Mantua et al. (1997). The IPO- index is defined according to Dai (2013) and Wang et
7
8
9 170 al. (2013). To emphasize the interannual variability, we remove the linear trends for
10
11 171 the aforementioned datasets. The effective degree of freedom (DOF) for the
12
13 172 significance test is calculated for each index (Trenberth, 1984; Bretherton et al.,
14
15 173 1999), which is almost the same as the original DOF.

16
17
18
19 174 Numerical experiments are performed with an atmospheric general circulation
20
21 175 model (AGCM), which is the 5th generation Max-Planck-Institute model, ECHAM
22
23 176 (v5.4) (Roeckner et al., 2003). The version we use is T63L19, with 1.875° for
24
25 177 horizontal resolution and 19 vertical levels. The SST forcing fields are derived from
26
27 178 the Atmospheric Model Intercomparison Project (AMIP) II Sea Surface Temperature
28
29 179 and Sea Ice Concentration Boundary Conditions. Three experiments are designed.
30
31
32
33 180 The control run is forced by the historical SST fields for 10 years from 1966 to 1975,
34
35 181 and the outcomes from the last 8 years are used to exclude the model spin-up. The
36
37 182 first sensitivity run (SR1) is forced by Dec.–Jan.–Feb. (DJF) SST differences
38
39 183 between the warm (normalized mega-ENSO index larger than 0.5) and cold
40
41 184 (normalized mega-ENSO index smaller than –0.5) mega-ENSO, which starts in 1966
42
43 185 and ends in 1975. The second sensitivity run (SR2) is similar to SR1, except for
44
45 186 removing the XNP SSTA from mega-ENSO.

46
47
48
49
50
51 187

52 53 54 188 **3. Interdecadal changes in the relationship between** 55 56 189 **mega-ENSO and WP/Aleutian Low** 57 58 59 60

1
2
3
4 190 Figure 2a presents the DJF SSTA pattern regressed against the mega-ENSO
5
6 191 index. It is seen that the spatial pattern of mega-ENSO, similar to that of ENSO, has
7
8
9 192 a larger spatial scale with negative SSTA in the western Pacific K-shape area and
10
11 193 positive SSTA in the eastern Pacific triangle area, in agreement with Wang et al.
12
13 194 (2013).

14
15
16 195 Using the mega-ENSO index, we found that there is a good connection between
17
18
19 196 mega-ENSO and the North Pacific atmospheric circulation (Fig. 2b), which displays a
20
21 197 westward extension of the Aleutian Low. The correlation coefficient (CC for short) is
22
23
24 198 -0.51 between mega-ENSO and the Aleutian Low, and is -0.34 between mega-ENSO
25
26 199 and the WP, both above the 99% confidence level based on the Student's t test.
27
28
29 200 Meanwhile, the NP index (NPI) and the WP index (WPI) are weakly correlated with
30
31 201 each other during the 56 years ($CC=-0.21$), indicating they are likely independent
32
33
34 202 atmospheric systems.

35
36 203 The 21-yr sliding correlations of the mega-ENSO index with the NP and WP
37
38
39 204 indices (Fig. 2c) show that there is a pronounced change of correlation during the
40
41 205 years of 1976–1978. In the earlier period (1957–1975), the mega-ENSO and WPI are
42
43 206 significantly correlated ($CC=-0.63$), while the mega-ENSO and NPI are not
44
45
46 207 ($CC=-0.18$). Thus, the early period is regarded as the coupling epoch between the WP
47
48
49 208 and mega-ENSO. In the latter period (1979–2012), the mega-ENSO and NPI are
50
51 209 significantly correlated ($CC=-0.66$), while the mega-ENSO and WPI are not
52
53
54 210 ($CC=-0.14$). Thus, latter period is regarded as the coupling epoch between the
55
56 211 Aleutian Low and mega-ENSO (Fig. 2d). This is in agreement with He et al. (2013),
57
58
59
60

1
2
3
4 212 who found the change in the relationship between the conventional ENSO and the
5
6 213 Asia-Pacific mid-latitude winter atmospheric circulation.
7

8
9 214 Before further analysis by using the mega-ENSO index, comparisons between
10
11 215 mega-ENSO and ENSO are made to explain why the mega-ENSO index is
12
13 216 introduced. First of all, we compare the pure mega-ENSO-related SSTA and 500 hPa
14
15 217 geopotential height (Z500) anomalies with the pure ENSO-related SSTA and Z500
16
17 218 anomalies from 1870 to 2012. The pure mega-ENSO winters are defined as those
18
19 219 when the normalized DJF mega-ENSO index is beyond ± 0.5 and in the meantime
20
21 220 the ENSO does not happen (Nino3.4 index is between -0.5 and 0.5). The pure
22
23 221 ENSOs are defined as those when the normalized DJF Nino3.4 index is beyond
24
25 222 ± 0.5 while the mega-ENSO doesn't happen (Fig. 3). This threshold provides
26
27 223 adequate numbers of mega-ENSO and ENSO cases to compare their spatial
28
29 224 structures. Figure 3a depicts the mega-ENSO-related SST difference (warm minus
30
31 225 cold years) in pure mega-ENSO years, showing strong negative SSTAs in a K-shape
32
33 226 area over the West Pacific and relatively weak positive SSTAs in a triangle region
34
35 227 over the East Pacific. It is distinctly different from that for the pure ENSO (Fig. 3b),
36
37 228 which shows significant SSTAs over the eastern and central tropical Pacific and a
38
39 229 weak gradient between the eastern and the western Pacific. Because of the different
40
41 230 types of SSTA forcing, the atmospheric responses are different. The Z500 anomalies
42
43 231 associated with a pure mega-ENSO (Fig. 3c) are significant at the mid-and-high
44
45 232 latitudes, but those corresponding to a pure ENSO (Fig. 3d) are significant in the
46
47 233 tropical region, with an opposite sign.
48
49
50
51
52
53
54
55
56
57
58
59
60

1
2
3
4 234 The power spectrum of the mega-ENSO and Nino3.4 indices are also compared.
5
6 235 Given that the period of the conventional ENSO is 3~5 years (NOAA/Climate
7
8
9 236 Prediction Center (CPC), online at
10
11 237 [http://www.cpc.ncep.noaa.gov/products/analysis_monitoring/ensocycle/ensocycle.sht](http://www.cpc.ncep.noaa.gov/products/analysis_monitoring/ensocycle/ensocycle.shtml)
12
13
14 238 ml), we removed the interannual signal (less than 5 years) from the mega-ENSO and
15
16 239 Nino3.4 indices using the Lanczos filter. Figure 3e indicates that the most significant
17
18
19 240 period of interdecadal mega-ENSO (ID) is about 15 years, which is absent for the
20
21 241 Nino3.4 (ID) (Fig. 3f) and PDO (Newman et al., 2003; fig. 3). Lastly, we find that the
22
23
24 242 Z500 anomaly response to a weak mega-ENSO is consistent with that to a strong one,
25
26 243 but such consistency does not exist for strong and weak conventional ENSOs. The
27
28
29 244 strong events are selected when the DJF mega-ENSO/Nino3.4 index values are
30
31 245 greater (less) than 1.0 (-1.0) standard deviation, and the weak events are selected
32
33
34 246 when the DJF mega-ENSO/Nino3.4 index values are between 0.5 (-1.0) and 1.0 (-0.5)
35
36 247 standard deviation. Composite analysis shows that the differences of the Z500
37
38
39 248 responses to strong mega-ENSO and to conventional ENSO in the two epochs are
40
41 249 quite similar (not shown). The Z500 anomalies in a weak mega-ENSO year is similar
42
43
44 250 to those in a strong mega-ENSO year (Figs. 4a and 4c). The Z500 anomaly response
45
46 251 to weak conventional ENSO changes from the early epoch, which is more similar to
47
48
49 252 an Aleutian Low (Fig. 4b), to the latter epoch, which shows no significant Aleutian
50
51 253 Low-like response (Fig. 4d). Thus, the association of WP/Aleutian Low with
52
53
54 254 mega-ENSO is more close and robust than that with conventional ENSO. In the
55
56 255 following, we analyze the changing SSTA related to the WP/Aleutian Low. In the
57
58
59
60

1
2
3
4 256 earlier epoch (Fig. 5a), the SSTA pattern regressed against the WP index resembles
5
6 257 that of the mega-ENSO SSTA pattern (spatial correlation coefficient (SCC) with Fig.
7
8
9 258 2a is -0.9), indicating that such an SSTA pattern can explain around 81% of the
10
11 259 mega-ENSO signal. A similar mega-ENSO-like SSTA pattern related to the Aleutian
12
13
14 260 Low is found in the latter epoch (Fig. 5d, $SCC=-0.96$). Such a close spatial
15
16 261 relationship can also be validated by a grid-by-grid comparison (Figs. 5e and 5f).
17
18
19 262 However, the correlation is greatly reduced between mega-ENSO and the WP index in
20
21 263 the latter epoch (Fig. 5b, $SCC=-0.44$), which is also the case for the correlation
22
23
24 264 between mega-ENSO and the Aleutian Low in the earlier epoch (Fig. 5c, $SCC=-0.45$).
25
26 265 It means that the SSTA pattern in Fig. 5b and Fig. 5c can only explain around 19%
27
28
29 266 and 20% of the mega-ENSO signal.

30
31 267 Therefore, there is a noticeable change in the linkage between the North Pacific
32
33
34 268 atmospheric circulation and mega-ENSO during the past 56 winters. To understand
35
36
37 269 the origin of such inter-decadal change, the spatial structure of mega-ENSO during
38
39 270 the two epochs will be examined in the following sections.

40
41 271

42 43 44 272 **4. Contrasting spatial structures of mega-ENSO in two** 45 46 273 **epochs**

47
48
49 274 Figure 6 compares the large-scale Z500 anomalies associated with mega-ENSO
50
51 275 during the two epochs. In general, the Z500 anomalies are symmetric about the
52
53
54 276 equator in the tropical zone during the two epochs. A major difference is located in the
55
56
57 277 mid-latitude North Pacific and the North Atlantic. In the earlier epoch (Fig. 6a), it is a

1
2
3
4 278 positive phase of the WP-like pattern over the North Pacific, with significantly high
5
6 279 pressure anomalies over the Kyushu Japan and low pressure anomalies over the
7
8
9 280 Kamchatka Peninsula and the western coast of North America. In the latter epoch (Fig.
10
11 281 6b), the high pressure anomalies over the Kyushu Japan disappear. Instead, there is a
12
13 282 deep Aleutian Low-like pattern over the Aleutian Islands and the Gulf of Alaska. In
14
15 283 addition, the Z500 anomalies exhibit a negative NAO-like pattern over the North
16
17 284 Atlantic in the earlier epoch but that disappears in the latter epoch, which was also
18
19 285 found by Wu and Zhang (2014) (their fig. 5). The 200 hPa geopotential height has a
20
21 286 similar feature as Z500, with major differences over the mid-and-high-latitudes as
22
23 287 well (not shown). We also regressed Z500 anomalies onto the PDO and IPO indices in
24
25 288 the two epochs and found that there is no significant difference. So, the PDO/IPO may
26
27 289 not be the key factor responsible for the inter-decadal variation of the WP and
28
29 290 Aleutian Low.
30
31
32
33
34
35

36 291 To explore the possible origin of the circulation differences, the SSTAs
37
38 292 associated with mega-ENSO are compared between the two epochs (Fig. 7). Both
39
40 293 epochs show a typical mega-ENSO pattern over the Pacific Ocean. The major
41
42 294 difference lies in the extra-tropical North Pacific (XNP, boxed area in Fig. 7), which
43
44 295 shows an east-west dipole pattern in the earlier epoch (Fig. 7a) and a quasi-single-sign
45
46 296 negative SSTA in the latter epoch (Fig. 7b). Such changes over the North Pacific are
47
48 297 accompanied with the changes over the North Atlantic (also seen in fig. 6 in Wu and
49
50 298 Zhang, 2014). The most prominent differences between the two epochs are in the
51
52 299 XNP and in the North Atlantic (Fig. 7c). An XNP index (XNPI) is defined as the
53
54
55
56
57
58
59
60

1
2
3
4 300 SSTA averaged within the boxed area (130°E–150°W, 15°N–40°N). Its correlation
5
6 301 with the mega-ENSO is –0.39 in the earlier epoch and –0.68 in the latter. Such an
7
8 302 interdecadal change in the North Pacific SSTA can also be discerned in the preceding
9
10 303 Sep.–Oct.–Nov. (SON) (not shown). In addition, the differences of the SSTA
11
12 304 associated with mega-ENSO and Nino3.4 between the two epochs are compared (not
13
14 305 shown). The results indicate that, with the same threshold, the SST differences caused
15
16 306 by the variation of mega-ENSO between the two epochs are more obvious and
17
18 307 persistent than that caused by the conventional ENSO. This implies that the
19
20 308 mega-ENSO is more closely related to the XNP SSTA than to the conventional
21
22 309 ENSO.
23
24
25
26
27

28
29 310 Figure 8 shows the difference of climatological SSTA between these two epochs
30
31 311 in SON and DJF. The patterns with significant SSTA over the North Pacific (Fig 8a
32
33 312 and 8b) are similar, except that the region with significant SSTA in DJF is larger than
34
35 313 that in SON. However, the east-west dipole SSTA pattern in the box region does not
36
37 314 accord with Fig. 7c. From Figs. 7 and 8, we conclude that the cooling of the XNP
38
39 315 SSTA from the former epoch to the latter epoch may not be caused by the change of
40
41 316 climatological SSTA, but the interdecadal change of mega-ENSO. As the connection
42
43 317 between mega-ENSO and the North Atlantic SSTA were discussed in Wu and Zhang
44
45 318 (2014), we will discuss the modulating effect of the XNP SSTA in the next part.
46
47
48
49
50

51 319

52 320 **5. The XNP modulation and numerical experiments**

53 321 **a. The XNP modulation**

54
55 322 Figure 9 depicts the different effects of mega-ENSO between the two epochs on
56
57
58
59
60

1
2
3
4 323 the XNPI. It can be seen that in the latter epoch (Fig. 9b) the XNPI is associated with
5
6 324 a mega-ENSO-like SSTA response as well as negative SSTAs over the extra-tropical
7
8
9 325 North Atlantic resembling the SSTA response to the mega-ENSO (Fig. 7b). Though
10
11 326 the XNP SSTA still exist, there is no significant mega-ENSO-like response in the
12
13
14 327 earlier epoch (Fig. 9a). These patterns indicate that the XNP has a synergistic effect on
15
16 328 the mega-ENSO during the 1979 to 2012, but such a characteristic is not obvious in
17
18
19 329 the years before 1975. Thus, we define 1957–1975 as the mega-ENSO without XNP
20
21 330 SSTA forcing period, and 1979–2012 as the mega-ENSO with XNP SSTA forcing
22
23
24 331 period. Next, the Z500 anomalies are regressed against XNPI (Fig. 10) to examine the
25
26 332 modulating effect of the XNP SSTA, which shows an evident Aleutian Low similar to
27
28
29 333 Fig. 6b. The possible reasons that may lead to the close connection between the XNP
30
31 334 and the Aleutian Low are suggested as follows: Comparing the wind anomalies over
32
33
34 335 the North Pacific in Fig. 7a and 7b, one of the major differences is the strength of the
35
36 336 westerly wind, which may be caused by the cooling of the XNP SSTA. In the former
37
38
39 337 epoch, because of the relatively warmer SSTA in the XNP region, the SST gradient
40
41 338 between the eastern and western North Pacific is weak, causing a weak upper sea
42
43
44 339 level pressure (SLP) gradient (Fig. 7d), which is against the generation of the
45
46 340 westerly. Following the interdecadal variability of mega-ENSO, the XNP SSTA
47
48
49 341 becomes cooler (Fig. 7c), making the zero line move westward (Fig. 7e), reinforcing
50
51 342 the upper SLP gradient and the westerly wind. This process is favorable for the
52
53
54 343 cyclone growth over the Gulf of Alaska, which further strengthens and maintains the
55
56 344 Aleutian Low. Meanwhile, the anticyclone over the Kamchatka Peninsula (Fig. 7c)

1
2
3
4 345 may be generated by the weakening westerly wind over the Okhotsk Sea, which
5
6 346 would obstruct the generation of the WP. Above all, the XNP SSTA cooling reinforces
7
8
9 347 the local westerly wind and weakens the Okhotsk Sea westerlies which may play a
10
11 348 great role in modulating the WP and Aleutian Low.

14 349 In order to exam whether the XNP SSTA could exert an effect without the
15
16 350 mega-ENSO. The partial-correlation is used to remove the mega-ENSO signal from
17
18
19 351 the XNP (Fig. 11). Compared to Fig. 10, the XNP SSTA can only excite a low
20
21
22 352 pressure, which is located to the west of the Aleutian Low in Fig. 11. The tropical
23
24
25 353 response does not exist, either. This suggests that the effect of XNP SSTA would take
26
27 354 place against the background of mega-ENSO. To verify whether the correlation
28
29 355 between the mega-ENSO and the WP/Aleutian Low depends on the XNP or not, the
30
31
32 356 partial-correlation is again used to remove the latter epoch XNP signal from the
33
34
35 357 mega-ENSO. The regressions of DJF Z500 anomalies against the mega-ENSO with
36
37 358 and without the XNP index signal removed are calculated (not shown). Their
38
39 359 difference (Fig. 12) shows that the WP pattern is more easily excited with the XNP
40
41
42 360 index signal removed compared to Fig. 6b. This confirms the previous assumption
43
44
45 361 that the emergence of the XNP SSTA against the background of mega-ENSO is
46
47 362 conducive to generating the Aleutian Low pattern atmospheric response. Otherwise,
48
49 363 the WP pattern atmospheric response will be excited.

50
51
52 364

55 365 **b. Numerical experiments**

1
2
3
4 366 To verify our hypothesis and elucidate the effect of an anomalous XNP SSTA
5
6 367 forcing on the modulation of WP and Aleutian Low, we perform the following
7
8
9 368 numerical experiments with the ECHAM5.4. The first experiment is the control run.
10
11 369 The second experiment is to impose a mega-ENSO type heating anomaly in the area
12
13
14 370 of (0°–360°E, 40°S–60°N). The third experiment is to remove the heating anomaly at
15
16 371 the XNP area against the background of mega-ENSO, which could eliminate the
17
18
19 372 diabatic heating effect of the XNP forcing. The control run and two sensitive
20
21 373 experiments are integrated for 10 years and the DJF is used to derive a reference state.
22
23
24 374 A 8-member ensemble (arithmetic) mean is constructed to reduce the uncertainties
25
26 375 arising from different initial conditions and the effect of mega-ENSO years. Here, the
27
28
29 376 control run can be regarded as the mega-ENSO-neutral condition, and the sensitive
30
31 377 run as the pure influence of mega-ENSO or XNP-neutral against the background of
32
33
34 378 mega-ENSO.

35
36 379 The model responses of Z500 and UV1000 to the mega-ENSO forcing are
37
38 380 shown in Fig. 13a (mega-ENSO forcing minus control run). Affected by the negative
39
40
41 381 XNP SSTA, the westerly flow is reinforced over the extra-tropical North Pacific (XNP)
42
43
44 382 following the strengthening of the North Pacific east-west SSTA gradient and an
45
46 383 Aleutian Low-like negative anomaly center is formed over the Gulf of Alaska and
47
48
49 384 Aleutian Islands at the upper troposphere, which is similar to the observation (Fig. 6b,
50
51 385 and wind field in Fig. 7b). However, after removing the XNP forcing against the
52
53
54 386 background of mega-ENSO, the westerly flow is moved northward, meanwhile, the
55
56 387 low pressure in the Aleutian region extends westward, which is a WP-like response
57
58
59
60

1
2
3
4 388 (Fig. 13b), similar to Fig. 6a and the wind field in Fig. 7a. In accordance with the
5
6 389 observation, Figure 13c shows that the AL or WP-like pattern would not respond to
7
8
9 390 the pure XNP SSTA forcing (the observe SSTA in the red box without mega-ENSO).
10
11 391 The numerical experiments results are quite consistent with the observations that the
12
13 392 mega-ENSO SSTA with the XNP signal is conducive to generating the Aleutian Low
14
15
16 393 at Z500. Otherwise, the WP pattern response will be excited by the mega-ENSO
17
18
19 394 without the XNP SSTA. And the location of the westerlies could be well reproduced
20
21 395 by ECHAM5.4, confirming our hypothesis that the XNP SSTA cooling reinforces the
22
23 396 east-west gradient and the local westerly wind, and meanwhile weakens the Okhotsk
24
25
26 397 Sea westerlies. The XNP against the background of mega-ENSO is the key factor in
27
28 398 modulating the WP and Aleutian Low.
29
30
31
32
33

34 400 **6. Conclusion and Discussion**

35
36 401 By using composite analysis, we found that the pure mega-ENSO and pure
37
38 402 ENSO SSTA pattern are different as well as their upper response, and the association
39
40 403 of the WP/Aleutian Low with mega-ENSO is more close and robust than that with
41
42 404 conventional ENSO. The power spectral analysis reveals that the mega-ENSO
43
44 405 contains more significant signal than conventional ENSO in the low-frequency band.
45
46
47
48

49 406 We found that the mega-ENSO –WP/Aleutian Low connection has experienced
50
51 407 a notable inter-decadal change in winter during the past decades. In 1957 –1975, there
52
53 408 was a significant correlation between the mega-ENSO and the WP, while the
54
55
56 409 mega-ENSO had a closer linkage with the Aleutian Low after 1979. So the
57
58
59
60

1
2
3
4 410 mega-ENSO actually exhibited intimate close connection with the WP in the former
5
6 411 epoch. Such a remarkable change in the mega-ENSO–WP/Aleutian Low connection
7
8
9 412 was related to the modulating effect of the XNP SSTA, which was caused by the
10
11 413 interdecadal change of mega-ENSO. Both numerical and theoretical evidence
12
13 414 confirmed that the XNP SSTA against the background of mega-ENSO reinforcing
14
15
16 415 westerly flow over the XNP region was conducive to exciting an Aleutian Low
17
18
19 416 atmospheric response, while a WP pattern was forced by the mega-ENSO without an
20
21 417 XNP SSTA which pushing the westerlies northward. Thus, the mega-ENSO, rather
22
23 418 than the ENSO/PDO/IPO, is a key factor responsible for the interdecadal variation of
24
25
26 419 the WP and Aleutian Low.

27
28
29 420 It should be pointed out here that the mega-ENSO is not the sole contributor to
30
31 421 the generation of the XNP SSTA. Although the correlation coefficient between the
32
33 422 mega-ENSO and XNP index reaches -0.63 , the mega-ENSO can only explain 39% of
34
35
36 423 the total XNP SST variance. For instance, the XNP SSTA is also related to the
37
38
39 424 extra-tropical North Atlantic SSTA (red boxed area in Fig. 14). And, some studies
40
41 425 have found the influence of the Atlantic SSTA on the Pacific Ocean. Ham et al. (2013)
42
43
44 426 pointed out that the tropical North Atlantic SST could be seen as a trigger for ENSO
45
46
47 427 events. The off-equatorial North Atlantic SSTA was linked to both the North Atlantic
48
49 428 variability (Watanabe and Kimoto, 1999; Okumura et al., 2001) and the ENSO (Klein
50
51 429 et al., 1999; Alexander and Scott, 2002). Thus, whether the Atlantic SSTA affects the
52
53
54 430 XNP directly or through the mega-ENSO is still unknown, and a better explanation of
55
56
57 431 the origin of XNP SSTA calls for further theoretical and numerical studies.
58
59
60

1
2
3
4 432 Last but not the least, many researches pointed out that the ENSO was still the
5
6 433 most predictable climatic signal (Kirtman and Schopf, 1998; Cheng et al., 2011), the
7
8
9 434 relations of ENSO to both the East Asian winter monsoon (EAWM) and the East
10
11 435 Asian summer monsoon (EASM) were shown to be modulated by the PDO (Chan and
12
13 436 Zhou, 2005; Wang et al., 2008) and IPO (Lee et al., 2013). As an integrated measure
14
15
16 437 of the ENSO, PDO and IPO, the mega-ENSO index was also used as a predictor to
17
18
19 438 predict the EASM leading to some good results (Wang et al, 2013; Wu and Yu, 2015).
20
21 439 Recently, Jia et al. (2015) showed that the second empirical orthogonal function (EOF)
22
23 440 of the surface air temperature (SAT) over East Asia was associated notably with
24
25
26 441 different circulation structures before and after the mid-1980s. In the North Pacific, a
27
28
29 442 large-scale low-pressure anomaly was associated with SAT-EOF2 before the
30
31 443 mid-1980s. However, a negative PNA-like pattern appeared after the mid-1980s
32
33
34 444 associated with SAT-EOF2. Our results show that the mega-ENSO may exert an
35
36 445 effect on the EAWM by exciting a PNA-like pattern (Aleutian Low) in the latter
37
38
39 446 epoch (Fig. 6b). Thus, the mega-ENSO may change its linking with the East Asian
40
41 447 winter monsoon or North American winter climate through modulating the North
42
43
44 448 Pacific atmospheric circulation. This highlights the importance of examining how the
45
46 449 mega-ENSO influences the North Pacific circulation patterns such as the WP or the
47
48
49 450 AL.

50
51
52 451

53
54 452 **Acknowledgements.** This work is jointly supported by the National Natural Science
55
56 453 Foundation of China (Grant Nos. 91437216 and 41575075), the Ministry of Science
57
58
59
60

1
2
3
4 454 and Technology of China (Grant Nos. 2015CB453201 and 2015CB953904) and the
5
6 455 Innovation project of Jiangsu Province (No. 1344051501004). The JRA-55 data used
7
8
9 456 here are freely available at <http://rda.ucar.edu/datasets/ds628.0/>, while the HadISST
10
11 457 data used here are freely available at
12
13 458 <http://www.metoffice.gov.uk/hadobs/hadisst/data/download.html>.

14
15
16 459
17
18
19 460
20
21 461
22
23
24 462
25
26
27
28
29
30
31
32
33
34
35
36
37
38
39
40
41
42
43
44
45
46
47
48
49
50
51
52
53
54
55
56
57
58
59
60

463 **References**

- 464 Alexander, M. A., and J. D. Scott, 2002: The influence of ENSO on air-sea interaction
465 in the Atlantic. *Geophys. Res. Lett.*, **29**(14), DOI: 10.1029/2001GL014347.
- 466 Anderson, B. T., C. F. Jason, M. C. Kim, and D. L. Emanuele, 2013: Extratropical
467 forcing of El Niño-Southern Oscillation asymmetry. *Geophys. Res. Lett.*,
468 **40**(18), 4916–4921.
- 469 Anderson, B. T., and C. P. Renelley, 2015: ENSO and non-ENSO induced charging
470 and discharging of the equatorial Pacific. *Clim. Dyn.*, DOI
471 10.1007/s00382-015-2472-x.
- 472 Barlow, M., S. Nigam, and E. H. Berbery, 2001: ENSO, Pacific decadal variability,
473 and U.S. summertime precipitation, drought, and stream flow. *J. Clim.*, **14**,
474 2105–2128.
- 475 Barnston, A. G., and R. E. Livezey, 1987: Classification, Seasonality and Persistence
476 of Low-Frequency Atmospheric Circulation Patterns. *Mon. Wea. Rev.*, **115**,
477 1083–1126.
- 478 Bjerknes, J., 1966: A possible response of the atmospheric Hadley circulation to
479 equatorial anomalies of ocean temperature. *Tellus*, **18**, 820–829.
- 480 Bjerknes, J., 1969: Atmospheric teleconnections from the equatorial Pacific. *Mon.*
481 *Wea. Rev.*, **97**, 163–172.
- 482 Bretherton, C. S., M. Widmann, V. P. Dymnikov, J. M. Wallace, and I. Blade, 1999:
483 Effective number of degrees of freedom of a spatial field. *J. Clim.*, **12**,
484 1990–2009.

- 1
2
3
4 485 Cane, M. A., S. E. Zebiak, and Y. Xue, 1995: Model studies of the long-term behavior
5
6 486 of ENSO, *Natural Climate Variability on Decade-Century Time Scales*. Edited
7
8
9 487 by D. G. Martinson et al., pp. 442–457, National Academy Press, Washington,
10
11 488 D.C.
- 12
13
14 489 Ceballos, L. I., E. D. Lorenzo, C. D. Hoyos, N. Schneider, and B. Taguchi, 2009:
15
16 490 North Pacific Gyre Oscillation Synchronizes Climate Fluctuations in the
17
18
19 491 Eastern and Western Boundary Systems. *J. Clim.*, **22**, 5163–5174.
- 20
21 492 Chan, J., C. L., and W. Zhou, 2005: PDO, ENSO and the early summer monsoon
22
23 493 rainfall over south China. *Geophys. Res. Lett.*, **32**, L08810,
24
25 494 doi:10.1029/2004GL022015.
- 26
27
28
29 495 Chang, C-P., Y. Zhang, and T. Li, 2000: Interannual and interdecadal variation of the
30
31 496 East Asian summer monsoon rainfall and tropical SSTs. Part 1: roles of the
32
33 497 subtropical ridge. *J. Clim.*, **13**, 4310–4325.
- 34
35
36 498 Charney, J. G., and J. Shukla, 1981: Predictability of monsoons. Edited by J. Lighthill
37
38 499 and R. P. Pearce at *Monsoon dynamics*, pp. 99–109, Cambridge University
40
41 500 Press, New York.
- 42
43
44 501 Cheng, Y., Y. Tang, and D. Chen, 2011: Relationship between predictability and
45
46 502 forecast skill of ENSO on various time scales. *J. Geophys. Res.*, **116**, C12006,
47
48 503 doi:10.1029/2011JC007249.
- 49
50
51 504 Dai, A. G., 2013: The influence of the inter-decadal Pacific oscillation on US
52
53 505 precipitation during 1923–2010. *Clim. Dyn.*, **41**, 633–646.
- 54
55
56 506 Deser, C., M. A. Alexander, and M. Timlin, 1996: Upper-ocean thermal variations in
57
58
59
60

- 1
2
3
4 507 the North Pacific during 1970–1991. *J. Clim.*, **9**, 1840–1855.
- 5
6 508 Deser, C., M. A. Alexander, and M. Timlin 1999: Evidence for a wind-driven
7
8 509 intensification of the Kuroshio Current extension from the 1970s to the 1980s. *J.*
9
10 510 *Clim.*, **12**, 1697–1706.
- 11
12
13 511 Ding, R., K. Ha, and J. Li, 2010: Interdecadal shift in the relationship between the
14
15 512 East Asian summer monsoon and the tropical Indian Ocean. *Clim. Dyn.*, **34**,
16
17 513 1059–1071. DOI: 10.1007/s00382-009-0555-2.
- 18
19
20 514 Folland, C. K., J. A. Renwick, M. J. Salinger, and A. B. Mullan, 2002: Relative
21
22 515 influences of the Interdecadal Pacific Oscillation and ENSO on the South
23
24 516 Pacific Convergence Zone. *Geophys. Res. Lett.*, **29**(13), 1643–1646.
- 25
26
27 517 Gong, D. Y., S. W. Wang, and J. H. Zhu, 2001: East Asian winter monsoon and
28
29 518 Arctic Oscillation. *Geophys. Res. Lett.*, **28**(10), 2073–2076.
- 30
31
32 519 Gu, D. F., and S. G. H. Philander, 1997: Interdecadal climate fluctuations that depend
33
34 520 on exchanges between the tropics and extratropics. *Science*, **275**, 805–807.
- 35
36
37 521 Graham, N. E., 1994: Decadal-scale climate variability in the tropical and North
38
39 522 Pacific during the 1970s and 1980s: Observations and model results. *Clim.*
40
41 523 *Dyn.*, **10**, 135–162.
- 42
43
44 524 Guilderson, T. P., and D. P. Schrag, 1998: Abrupt shift in subsurface temperatures in
45
46 525 the tropical Pacific associated with changes in El Niño. *Science*, **281**, 240–243.
47
48 526 DOI: 10.1126/science.281.5374.240.
- 49
50
51 527 Ham, Y. G., J. S. Kug, J. Y. Park, and F. F. Jin, 2013: Sea surface temperature in the
52
53 528 north tropical Atlantic as a trigger for El Niño/Southern Oscillation events.
54
55
56
57
58
59
60

- 1
2
3
4 529 Nature. Geos., **6**, 112–116.
- 5
6 530 Hanawa, K., S. Ishizaki, and Y. Tanimoto, 1996: Strengthening of wintertime
7
8 531 midlatitude westerlies over the North Pacific since mid 1970s. *J. Meteor. Soc.*
9
10 532 *Jpn.*, **74**, 715–721.
- 11
12 533 He, S. P., and H. J. Wang, 2013a: Oscillating relationship between the East Asian
13
14 534 winter monsoon and ENSO. *J. Clim.*, **26**, 9819–9838.
- 15
16 535 He, S. P., H. J. Wang, and J. P. Liu, 2013b: Changes in the Relationship between
17
18 536 ENSO and Asia Pacific Midlatitude Winter Atmospheric Circulation. *J. Clim.*,
19
20 537 **26**, 3377–3393.
- 21
22 538 Horel, J. D., and J. M. Wallace, 1981: Planetary-scale atmospheric phenomena
23
24 539 associated with the Southern Oscillation. *Mon. Wea. Rev.*, **109**, 813–829.
- 25
26 540 Hsu, H. H., and J. D. Wallace, 1985: Vertical structure of winter-time teleconnection
27
28 541 patterns. *J. Atmos. Sci.*, **42**, 1693–1710.
- 29
30 542 Jia, X., H. Lin, and J. Ge, 2015: The interdecadal change of ENSO impact on
31
32 543 wintertime East Asian climate. *J. Geophys. Res. Atmos.*, **120**, 11,918–11,935,
33
34 544 doi:10.1002/2015JD023583.
- 35
36 545 Jin, F. F., J. D. Neelin, and M. Ghil, 1994: El Niño on the devil’s staircase: annual
37
38 546 subharmonic steps to chaos. *Science*, **264**, 70–72.
- 39
40 547 Kim, B.-H., and K.-J. Ha, 2015: Observed changes of global and western Pacific
41
42 548 precipitation associated with global warming SST mode and mega-ENSO SST
43
44 549 mode. *Clim. Dyn.*, doi:10.1007/s00382-015-2524-2.
- 45
46 550 Kirtman, B. P., and P. S. Schopf, 1998: Decadal variability in ENSO predictability
47
48
49
50
51
52
53
54
55
56
57
58
59
60

- 1
2
3
4 551 and prediction. *J. Climate*, **11**, 2804–2822.
- 5
6 552 Klein, S. A., B. J. Soden, and N. C. Lau, 1999: Remote sea surface temperature
7
8 553 variations during ENSO: Evidence for a tropical atmospheric bridge. *J. Clim.*,
9
10 554 **12**, 917–932.
- 11
12
13 555 Kobayashi, S., Y. Ota, Y. Harada, A. Ebita, M. Moriya, H. Onoda, K. Onogi, H.
14
15
16 556 Kamahori, C. Kobayashi, H. Endo, K. Miyaoka, and K. Takahashi, 2015: The
17
18 557 JRA-55 Reanalysis: General Specifications and Basic Characteristics. *J. Meteor.*
19
20 558 *Soc. Jpn.*, **93**(1), 5–48.
- 21
22
23 559 Kodera, K., 1998: Consideration of the origin of the different midlatitude atmospheric
24
25 560 responses among El Niño events. *J. Meteor. Soc. Jpn.*, **76**, 347–361.
- 26
27
28 561 Latif, M., and T. P. Barnett, 1994: Causes of decadal climate variability over the
29
30 562 North Pacific and North America. *Science*, **266**, 634–637.
- 31
32
33 563 Latif, M., and T. P. Barnett, 1996: Decadal Climate Variability over the North Pacific
34
35 564 and North America: Dynamics and Predictability. *J. Clim.*, **9**, 2407–2423.
- 36
37
38 565 Lee, S.-S., S.-H. Kim, J.-G. Jhun, K.-J. Ha, and Y.-W. Seo, 2013: Robust warming
39
40 566 over East Asia during boreal winter monsoon and its possible causes. *Env. Res.*
41
42 567 *Lett.*, **8**(3), 34001, doi:10.1088/1748-9326/8/3/034001.
- 43
44
45 568 Linkin, M. E., and S. Nigam, 2008: The North Pacific Oscillation–West Pacific
46
47 569 Teleconnection Pattern: Mature-Phase Structure and Winter Impacts. *J. Clim.*,
48
49 570 **21**, 1979–1997.
- 50
51
52 571 Mantua, N. J., S. R. Hare, Y. Zhang, J. M. Wallace, R. C. A. Francis, 1997: Pacific
53
54 572 interdecadal climate oscillation with impacts on salmon production. *Bull. Amer.*

- 1
2
3
4 573 Meteor. Soc., **78**, 1069–1079.
- 5
6 574 Maslanik, J. A., M. C. Serreze, and R. G. Barry, 1996: Recent decreases in Arctic
7
8 575 summer ice cover and linkages to atmospheric circulation anomalies. *Geophys.*
9
10 576 *Res. Lett.*, **23**, 1677–1680.
- 11
12
13 577 Mo, K. C., and R. E. Livezey, 1986: Tropical-extratropical geopotential height
14
15 578 teleconnections during the Northern Hemisphere winter. *Mon. Wea. Rev.*, **114**,
16
17 579 2488–2515.
- 18
19
20 580 Neelin, J. D., D. S. Battisti, A. C. Hirst, F. F. Jin, Y. Wakata, T. Yamagata, and S.
21
22 581 Zebiak, 1998: ENSO theory. *J. Geophys. Res.*, **103**(C7), 14261–14290.
- 23
24
25 582 Newman, M. G. P. Compo, and M. A. Alexander, 2003: ENSO-Forced Variability of
26
27 583 the Pacific Decadal Oscillation. *J. Clim.*, **16**, 3853–3857.
- 28
29
30 584 Nigam, 2003: Teleconnections. *Encyclopedia of Atmospheric Sciences*. Edited by J.
31
32 585 R. Holton et al., pp. 2243–2269, Academic Press.
- 33
34
35 586 Oshika, M., Y. Tachibana, and T. Nakamura, 2014: Impact of the winter North
36
37 587 Atlantic Oscillation (NAO) on the Western Pacific (WP) pattern in the
38
39 588 following winter through Arctic sea ice and ENSO: part I—observational
40
41 589 evidence. *Clim. Dyn.*, DOI: 10.1007/s00382-014-2384-1.
- 42
43
44 590 Okumura, Y., S-P. Xie, A. Numaguti, and Y. Tanimoto, 2001: Tropical Atlantic
45
46 591 air-sea interaction and its influence on the NAO. *Geophys. Res. Lett.*, **28**,
47
48 592 1507–1510.
- 49
50
51 593 Overland, J. E., J. M. Adams, and N. A. Bond, 1999: Decadal Variability of the
52
53 594 Aleutian Low and Its Relation to High-Latitude Circulation. *J. Clim.*, **12**,

- 1
2
3
4 595 1542–1548.
- 5
6 596 Philander, S. G. H. 1981: The response of Equatorial Oceans to a relaxation of the
7
8
9 597 trade winds. *J. Phys. Oceanogr.*, **11**(2), 176–189.
- 10
11 598 Rayner, N. A., D. E. Parker, E. B. Horton, C. K. Folland, L. V. Alexander, D. P.
12
13 599 Rowell, E. C. Kent, and A. Kaplan, 2003: Global analyses of sea surface
14
15 600 temperature, sea ice, and night marine air temperature since the late nineteenth
16
17 601 century. *J. Geophys. Res.*, **108**(4407), DOI: 10.1029/2002JD002670.
- 18
19 602 Roeckner, E., G. Bäuml, and et al., 2003: The atmospheric general circulation model
20
21 603 ECHAM5: Part I: Model description. Max Planck Institute Rep. 349, 140 pp.
- 22
23 604 Rogers, J. C., 1981: The North Pacific Oscillation. *J. Climatol.* **1**, 39–58.
- 24
25 605 Ropelewski, C. F., and M. S. Halpert, 1986: North American Precipitation and
26
27 606 Temperature Patterns Associated with the El Niño/Southern Oscillation
28
29 607 (ENSO). *Mon. Wea. Rev.*, **114**, 2352–2362.
- 30
31 608 Trenberth, K. E., 1984: Some effects of finite sample size and persistence on
32
33 609 meteorological statistics. Part I: Autocorrelations. *Mon. Wea. Rev.*, **112**,
34
35 610 2359–2368.
- 36
37 611 Trenberth, K. E., 1990: Recent observed interdecadal climate changes in the Northern
38
39 612 Hemisphere, *Bull. Amer. Meteor. Soc.*, **71**, 988–993.
- 40
41 613 Trenberth, K. E., 1991: Recent climate changes in the Northern Hemisphere. DOE
42
43 614 Workshop, 8-12 May, edited by M. Schlesinger at Greenhouse-gas-induced
44
45 615 climate change: a critical appraisal of simulations and observations, pp.
46
47 616 377–390, Elsevier, Amsterdam.
- 48
49
50
51
52
53
54
55
56
57
58
59
60

- 1
2
3
4 617 Trenberth, K. E., and J. W. Hurrell, 1994: Decadal atmosphere-ocean variations in the
5
6 618 Pacific. *Clim. Dyn.*, **9**, 303–319.
7
8
9 619 Trenberth, K. E., J. G. Olson, and W. G. Large, 1989: Aglobal ocean wind stress
10
11 620 climatology based on ECMWF analyses. NCAR Technical Note
12
13 621 NCAR/TN-338+STR, DOI: 10.5065/D6ST7MR9.
14
15
16 622 Walker, G., and E. Bliss (1932), World weather. V. *Mem. Roy. Meteor. Soc.*, **4**,
17
18 623 53–84.
19
20
21 624 Wallace, J. M., and D. Gutzler, 1981: Teleconnections in the geopotential height field
22
23 625 during the Northern Hemisphere winter. *Mon. Wea. Rev.*, **109**, 784–812.
24
25
26 626 Wang, B., R. G. Wu, and X. H. Fu, 2000: Pacific-East Asia teleconnection: how does
27
28 627 ENSO affect East Asian climate? *J. Clim.*, **13**, 1517–1536.
29
30
31 628 Wang, B., Z. W. Wu, J. P. Li, J. Liu, C-P. Chang, Y. H. Ding, and G. X. Wu, 2008:
32
33 629 How to measure the strength of the East Asian summer monsoon? *J. Clim.*, **21**,
34
35 630 4449–4463.
36
37
38 631 Wang, B., J. Liu, H. J. Kim, P. J. Webster, S. Y. Yim, and B. Q. Xiang, 2013:
39
40 632 Northern Hemisphere summer monsoon intensified by mega-El Niño/southern
41
42 633 oscillation and Atlantic multidecadal oscillation. *Proc. Natl. Acad. Sci. USA*, **14**,
43
44 634 5347–5352.
45
46
47 635 Wang, B., et al., 2015: Rethinking Indian monsoon rainfall prediction in the context
48
49 636 of recent global warming. *Nat. Commun.*, doi:10.1038/ncomms8154.
50
51
52 637 Wang, L., W. Chen, and R. Huang, 2008: Interdecadal modulation of PDO on the
53
54 638 impact of ENSO on the East Asian winter monsoon. *Geophys. Res. Lett.*, **35**,
55
56
57
58
59
60

- 1
2
3
4 639 L20702, doi:10.1029/2008GL035287.
5
6 640 Watanabe, M., and M. Kimoto, 1999: Tropical-extratropical connection in the
7
8 641 Atlantic atmosphere-ocean variability. *Geophys. Res. Lett.*, **26**, 2247–2250.
9
10
11 642 Wu, Z., and J. Li, 2008: Prediction of the Asian-Australian monsoon inter-annual
12
13 643 variations with the grid-point atmospheric model of IAP LASG (GAMIL), *Adv.*
14
15 644 *Atmos. Sci.*, **25**(3), 387–394.
16
17
18 645 Wu, Z., and J. Li, 2009: Seasonal prediction of the global precipitation annual modes
19
20 646 with the grid-point atmospheric model of IAP LASG (GAMIL). *Acta. Meteor.*
21
22 647 *Sinica.*, **23**(4), 428–437.
23
24
25 648 Wu, Z., and H. Lin, 2012: Interdecadal variability of the ENSO-North Atlantic
26
27 649 Oscillation connection in boreal summer. *Quart. J. Roy. Meteor. Soc.*, **138**,
28
29 650 1668–1675.
30
31
32 651 Wu, Z., B. Wang, J. Li, and F. F. Jin, 2009: An empirical seasonal prediction model
33
34 652 of the East Asian summer monsoon using ENSO and NAO. *J. Geophys. Res.*,
35
36 653 **114**, D18120. DOI: 10.1029/2009JD011733.
37
38
39 654 Wu, Z., and P. Zhang, 2014: Interdecadal variability of the mega-ENSO-NAO
40
41 655 synchronization in winter. *Clim. Dyn.*, DOI: 10.1007/s00382-014-2361-8.
42
43
44 656 Wu, Z., and L. Yu, 2015: Seasonal prediction of the East Asian summer monsoon
45
46 657 with a partial-least square model. *Clim. Dyn.*, doi:10.1007/s00382-015-2753-4.
47
48
49 658 Wyrski, K., 1975: The dynamic response of the equatorial Pacific ocean to
50
51 659 atmospheric forcing. *J. Phy. Oceanogr.*, **5**, 572–584.
52
53
54 660 Yukimoto, S. J., E. Masahiro, K. Yoshiteru, K. Akio, M. Tatsuo, and N. Akira, 2000:
55
56
57
58
59
60

- 1
2
3
4 661 ENSO-like interdecadal variability in the Pacific Ocean as simulated in a
5
6 662 coupled general circulation model, *J. Geophys. Res.*, **15(C6)**, 13945–13963.
7
8
9 663 Yukimoto, S. et al., 1996: Interannual and interdecadal variabilities in the Pacific in
10
11 664 an MRI coupled GCM. *Clim. Dyn.*, **12**, 667–683.
12
13
14 665 Zhang, R. H., A. Sumi, and M. Kimoto, 1996: Impact of El Niño on the East Asia
15
16 666 Monsoon: a diagnostic study of the ‘86/87 and ‘91/92 events. *J. Meteor. Soc.*
17
18 667 *Jpn.*, **74**, 49–62.
19
20
21 668 Zhang, Z., D. Gong, M. Hu, D. Guo, X. He, and Y. Lei, 2009: Anomalous winter
22
23 669 temperature and precipitation events in southern China. *J. Geogr. Sci.* **19(4)**,
24
25
26 670 471–488.
27
28
29 671

672 **Figure Captions**

673 FIG. 1. December–January–February (DJF) 500-hPa geopotential height (Z500)
674 anomalies regressed against (a) the North Pacific (NP) index (contours in units of
675 hPa) (b) the West Pacific (WP) index from 1957 to 2012. The shaded areas
676 exceed the 95% confidence level based on the Student's t test.

677 FIG. 2. (a) DJF sea surface temperature anomaly (SSTA) (b) Z500 anomalies
678 regressed against the mega-ENSO index (contours in units of $^{\circ}\text{C}$ and hPa) during
679 1957 to 2012. The red lines outline the eastern Pacific triangle and western
680 Pacific K-shape regions where the mega-ENSO index is defined. The shaded
681 areas exceed the 95% confidence level based on the Student's t test. (c) The
682 21-yr sliding correlation of the mega-ENSO index with the WP index (red curve)
683 and the NPI (blue curve). The horizontal dashed line indicates the values exceed
684 the 95% confidence level based on the Student's t test. (d) Time series of the
685 normalized NPI (black curve), WPI (red curve) and mega-ENSO index (bar) in
686 DJF for the period of 1957–2012. Yellow and green shaded area denotes
687 transition period.

688 FIG. 3. DJF SSTA (contours in units of $^{\circ}\text{C}$) composite difference between the warm
689 and cold (a) mega-ENSO with neutral conventional ENSO years (b)
690 conventional ENSO with neutral mega-ENSO years, (c) (d) is the same as (a) (b),
691 except for Z500 (contours in units of hPa). The dotted areas plotted in exceed
692 90% confidence level. And the power spectrum of (e) mega-ENSO index from
693 1901 to 2010 after extracting the inter-decadal signal (mega-ENSO (ID)), (f)

1
2
3
4 694 Nino3.4 (ID). The red dash-lines from (e) to (f) represent spectrum of red noise
5
6 695 at 95% level.
7

8
9 696 FIG. 4. DJF Z500 (shaded units of hPa) composite difference between the warm and
10
11 697 cold strong (a) mega-ENSO (b) Nino3.4 years from 1957 to 1975, (c) (d) is the
12
13 698 same as (a) (b), except for 1979–2012. A weak year refers to that of a DJF
14
15 699 mega-ENSO/Nino3.4 index value between 0.5 (–1) and 1 (–0.5) times standard
16
17 700 deviation.
18
19

20
21 701 FIG. 5. 1957–1975 and 1979–2012 DJF SSTA (contours in units of °C) pattern
22
23 702 regressed against the WP index (a) and (b), NP index (c) and (d). The shaded
24
25 703 areas exceed the 90% confidence level. The scatter plot compares the SSTA
26
27 704 spatial pattern regressed against WP (e), NP (f) index with the SSTA spatial
28
29 705 pattern regressed against mega-ENSO.
30
31
32

33
34 706 FIG. 6. The DJF Z500 (contours in units of hPa) pattern regressed against the
35
36 707 mega-ENSO for the (a) 1957–1975 and (b) 1979–2012 period. The shaded areas
37
38 708 exceed the 95% confidence level.
39

40
41 709 FIG. 7. DJF SSTA (contours in units of °C) and 1000 hPa wind anomalies (vectors in
42
43 710 units of m/s) regressed against the normalized mega-ENSO index for (a)
44
45 711 1957–1975; (b) 1979–2012; (c) (b)–(a). (e), (f) are the DJF sea level pressure
46
47 712 (SLP) anomalies regressed against the normalized mega-ENSO index at
48
49 713 1957–1975, 1979–2012. The shaded areas or wind vectors plotted in (a), (b), (e)
50
51 714 and (f) exceed 95% confidence level, while those in (c) indicate SSTAs above
52
53 715 0.18°C or below –0.18°C, wind vectors above 0.8 m/s. The SSTA averaged in
54
55
56
57
58
59
60

1
2
3
4 716 the purple box (130°E – 150°W , 15°N – 40°N) is defined as an extra-tropical North
5
6 717 Pacific (XNP) index (XNPI).

7
8
9 718 FIG. 8. (a) SON and (b) DJF climatology SST difference between 1979–2012 and
10
11 719 1957–1975. The dotted and forked areas represent exceed 95% confidence level.
12
13
14 720 The purple box denotes XNP area.

15
16 721 FIG. 9. The DJF SSTA (contours in units of K) pattern regressed against the XNPI for
17
18 722 the (a) 1957–1975 and (b) 1979–2012 period. The shaded areas exceed the 95%
19
20
21 723 confidence level.

22
23
24 724 FIG. 10. DJF Z500 anomalies regressed against the XNP (contours in unit of hPa).
25
26 725 The shaded areas exceed the 95% confidence level.

27
28
29 726 FIG. 11. Same as Figure 9, except for partial regressed against the XNP with the
30
31 727 mega-ENSO index signal removed. The shaded areas exceed the 95% confidence
32
33
34 728 level.

35
36 729 FIG. 12. The regressions of DJF Z500 anomalies against the mega-ENSO with and
37
38
39 730 without the XNP index signal removed. The shaded areas indicate above 4 hPa or
40
41 731 below -4 hPa.

42
43
44 732 FIG. 13. (a) DJF Z500 (contours in units of hPa) and UV1000 (vectors in units of m/s)
45
46 733 responses in the ECHAM5 regarding a difference between mega-ENSO forcing
47
48
49 734 and control run. (b) Same as (a) but with XNP forcing removed, (c) with pure
50
51 735 XNP forcing without mega-ENSO. The shaded areas indicate above 2 hPa or
52
53
54 736 below -2 hPa, wind vectors above 0.8 m/s.

55
56
57 737

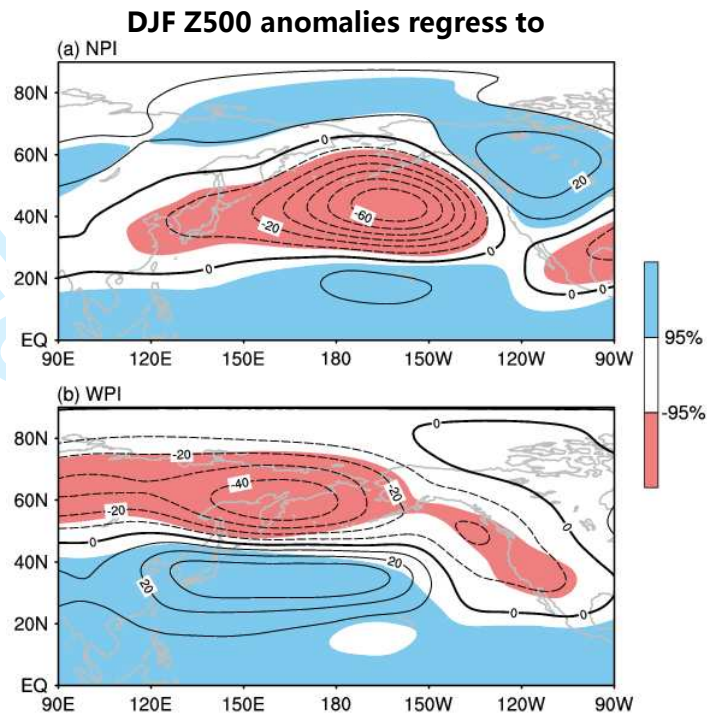
1
2
3
4 738 FIG. 14. (a) DJF (b) SON and (c) JJA SSTA (contours in units of °C) regressed against
5
6 739 the XNP index. The shaded areas exceed 95% confidence level. And the red box
7
8
9 740 denotes XNA SSTA.

10
11 741

12
13 742
14
15
16
17
18
19
20
21
22
23
24
25
26
27
28
29
30
31
32
33
34
35
36
37
38
39
40
41
42
43
44
45
46
47
48
49
50
51
52
53
54
55
56
57
58
59
60

For Peer Review Only

743



744

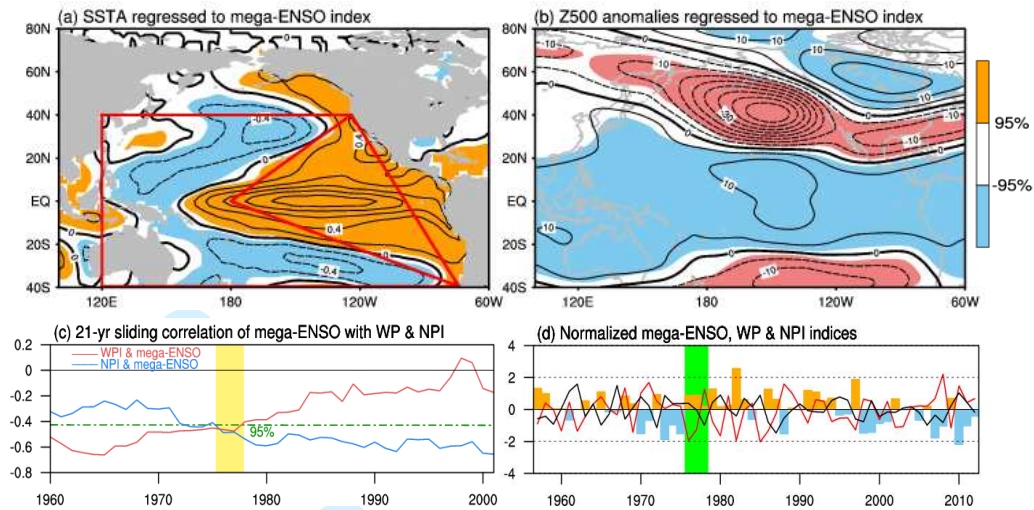
745

746

747 FIG. 1. December–January–February (DJF) 500-hPa geopotential height (Z500)
748 anomalies regressed against (a) the North Pacific (NP) index (contours in units of hPa)
749 (b) the West Pacific (WP) index from 1957 to 2012. The shaded areas exceed the
750 95% confidence level based on the Student's t test.

751

752



753

754

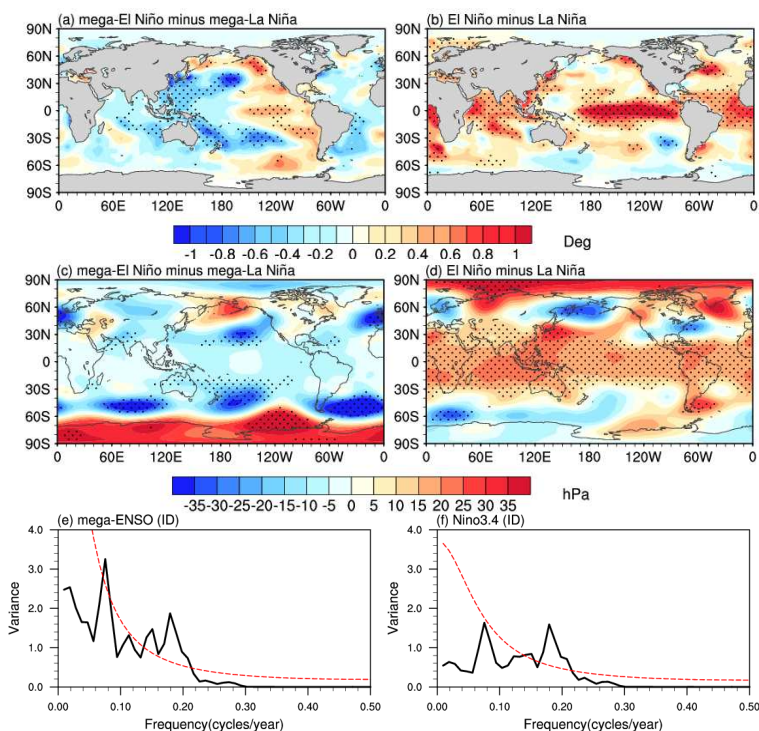
755

756 FIG. 2. (a) DJF sea surface temperature anomaly (SSTA) (b) Z500 anomalies
 757 regressed against the mega-ENSO index (contours in units of $^{\circ}\text{C}$ and hPa) during
 758 1957 to 2012. The red lines outline the eastern Pacific triangle and western Pacific
 759 K-shape regions where the mega-ENSO index is defined. The shaded areas exceed the
 760 95% confidence level based on the Student's t test. (c) The 21-yr sliding correlation of
 761 the mega-ENSO index with the WP index (red curve) and the NPI (blue curve). The
 762 horizontal dashed line indicates the values exceed the 95% confidence level based on
 763 the Student's t test. (d) Time series of the normalized NPI (black curve), WPI (red
 764 curve) and mega-ENSO index (bar) in DJF for the period of 1957–2012. Yellow and
 765 green shaded area denotes transition period.

766

767

768



769

770

771

772 FIG. 3. DJF SSTA (contours in units of $^{\circ}\text{C}$) composite difference between the warm
 773 and cold (a) mega-ENSO with neutral conventional ENSO years (b) conventional
 774 ENSO with neutral mega-ENSO years, (c) (d) is the same as (a) (b), except for Z500
 775 (contours in units of hPa). The dotted areas plotted in exceed 90% confidence level.
 776 And the power spectrum of (e) mega-ENSO index from 1901 to 2010 after extracting
 777 the inter-decadal signal (mega-ENSO (ID)), (f) Nino3.4 (ID). The red dash-lines from
 778 (e) to (f) represent spectrum of red noise at 95% level.

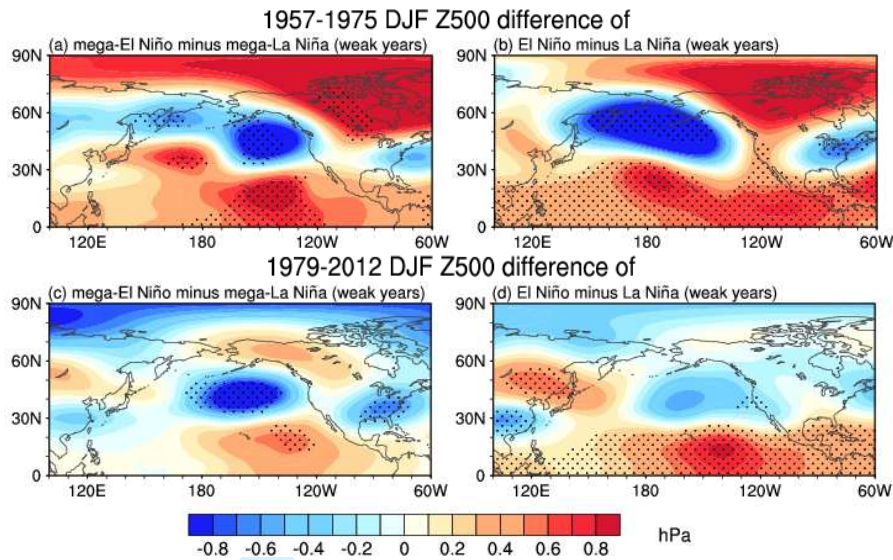
779

780

781

782

783



784

785

786

787 FIG. 4. DJF Z500 (shaded units of hPa) composite difference between the warm and

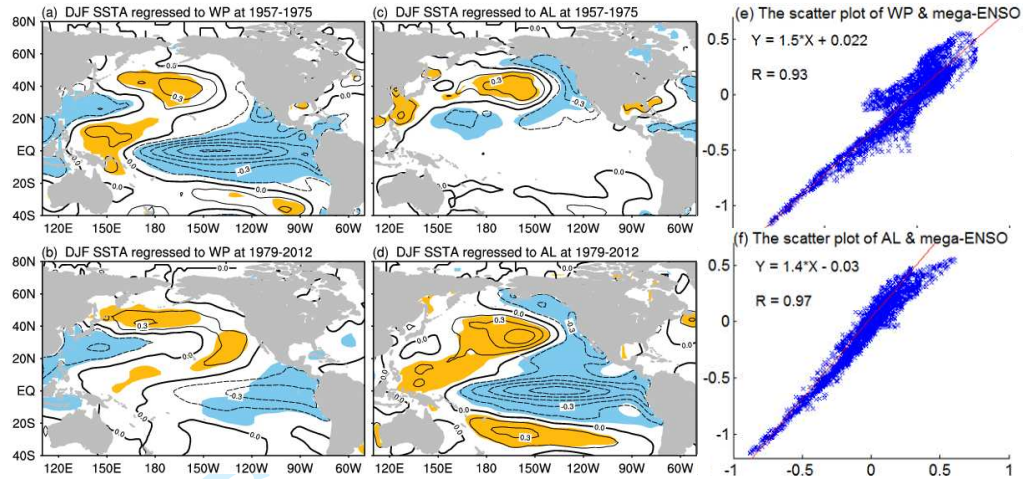
788 cold strong (a) mega-ENSO (b) Niño3.4 years from 1957 to 1975, (c) (d) is the same

789 as (a) (b), except for 1979–2012. A weak year refers to that of a DJF

790 mega-ENSO/Niño3.4 index value between 0.5 (–1) and 1 (–0.5) times standard

791 deviation.

792



793

794

795

796 FIG. 5. 1957–1975 and 1979–2012 DJF SSTA (contours in units of °C) pattern

797 regressed against the WP index (a) and (b), NP index (c) and (d). The shaded areas

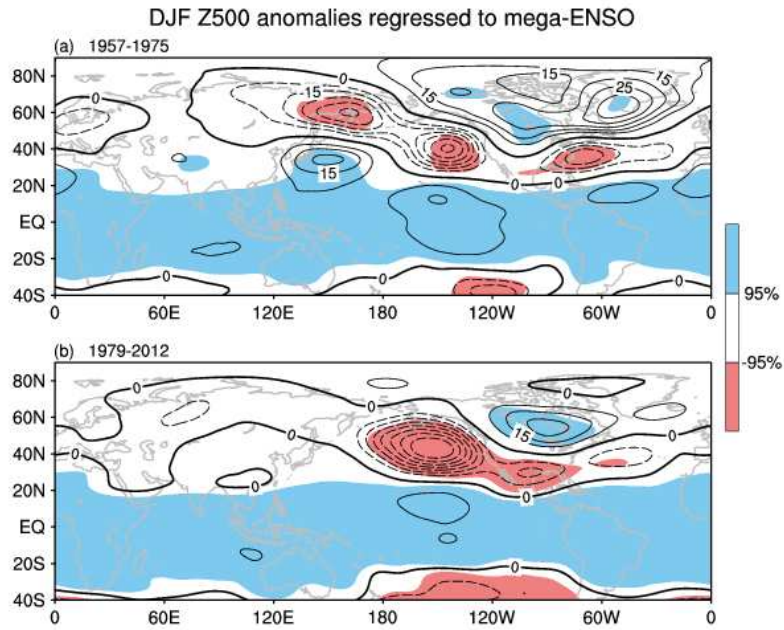
798 exceed the 90% confidence level. The scatter plot compares the SSTA spatial pattern

799 regressed against WP (e), NP (f) index with the SSTA spatial pattern regressed against

800 mega-ENSO.

801

802



803

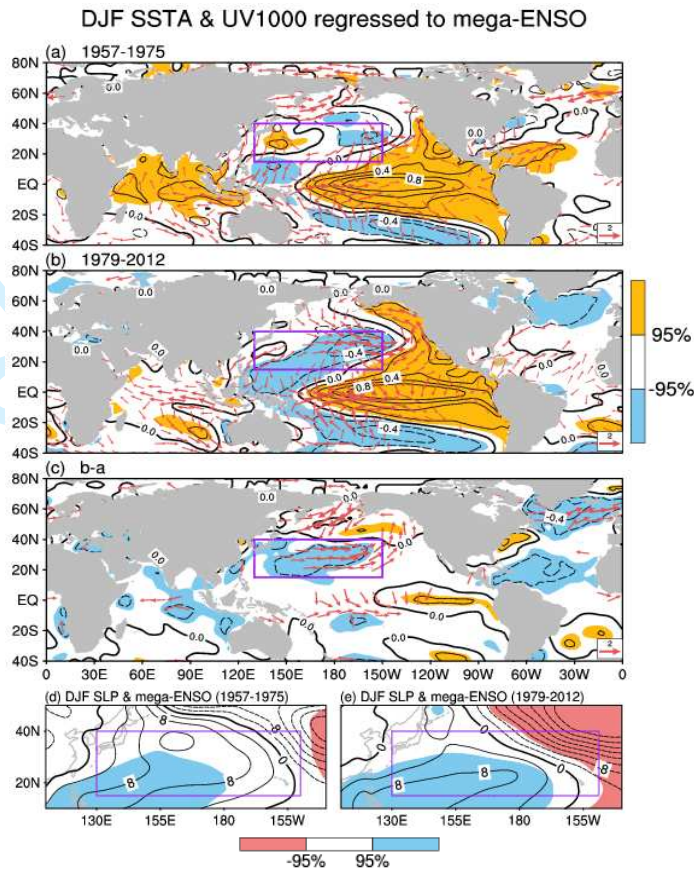
804

805

806 FIG. 6. The DJF Z500 (contours in units of hPa) pattern regressed against the
807 mega-ENSO for the (a) 1957–1975 and (b) 1979–2012 period. The shaded areas
808 exceed the 95% confidence level.

809

810



811

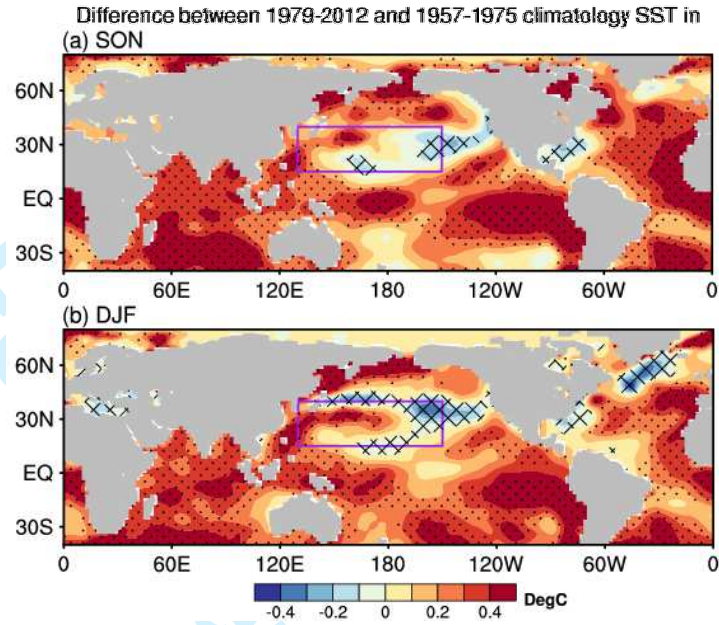
812

813

814 FIG. 7. DJF SSTA (contours in units of $^{\circ}\text{C}$) and 1000 hPa wind anomalies (vectors in
 815 units of m/s) regressed against the normalized mega-ENSO index for (a) 1957–1975;
 816 (b) 1979–2012; (c) (b)–(a). (e), (f) are the DJF sea level pressure (SLP) anomalies
 817 regressed against the normalized mega-ENSO index at 1957–1975, 1979–2012. The
 818 shaded areas or wind vectors plotted in (a), (b), (e) and (f) exceed 95% confidence
 819 level, while those in (c) indicate SSTAs above 0.18°C or below -0.18°C , wind vectors
 820 above 0.8 m/s . The SSTA averaged in the purple box (130°E – 150°W , 15°N – 40°N) is
 821 defined as an extra-tropical North Pacific (XNP) index (XNPi).

822

823



824

825

826

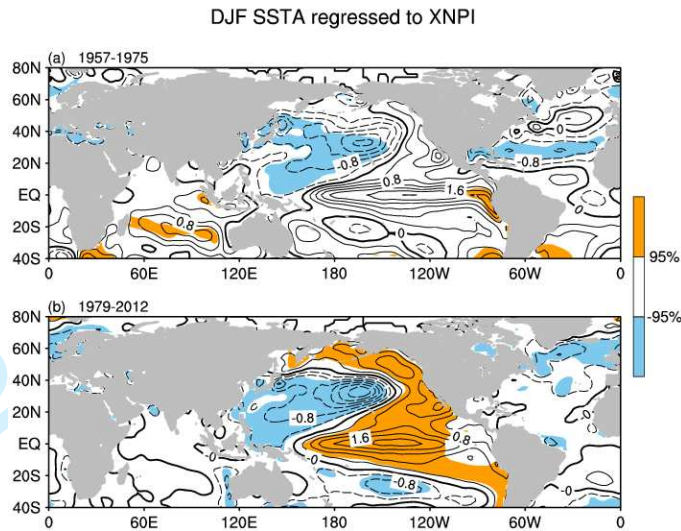
827 FIG. 8. (a) SON and (b) DJF climatology SST difference between 1979–2012 and

828 1957–1975. The dotted and forked areas represent exceed 95% confidence level. The

829 purple box denotes XNP area.

830

831



832

833

834

835 FIG. 9. The DJF SSTA (contours in units of K) pattern regressed against the XNPI for
836 the (a) 1957–1975 and (b) 1979–2012 period. The shaded areas exceed the 95%
837 confidence level.

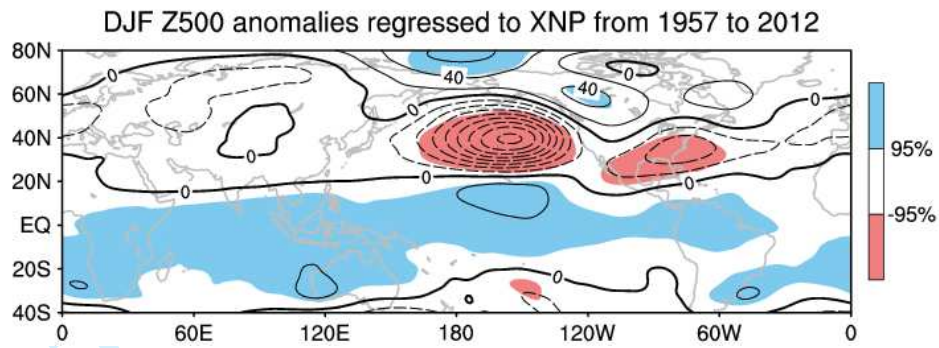
838

839

840

841

842



843

844

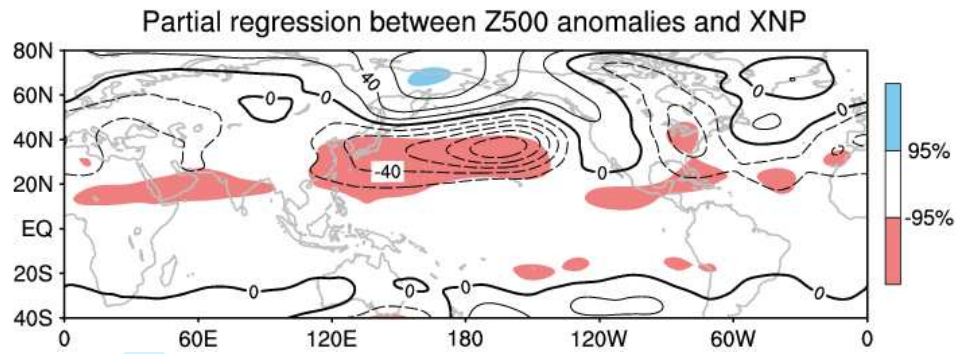
845

846 FIG. 10. DJF Z500 anomalies regressed against the XNP (contours in unit of hPa).

847 The shaded areas exceed the 95% confidence level.

848

849



850

851

852

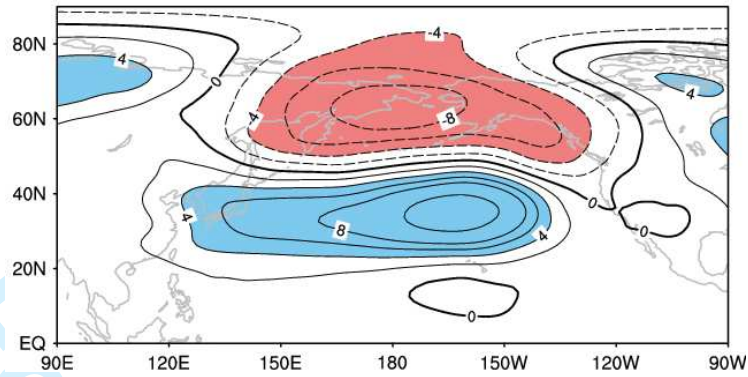
853 FIG. 11. Same as Figure 9, except for partial regressed against the XNP with the

854 mega-ENSO index signal removed. The shaded areas exceed the 95% confidence

855 level.

856

857



858

859

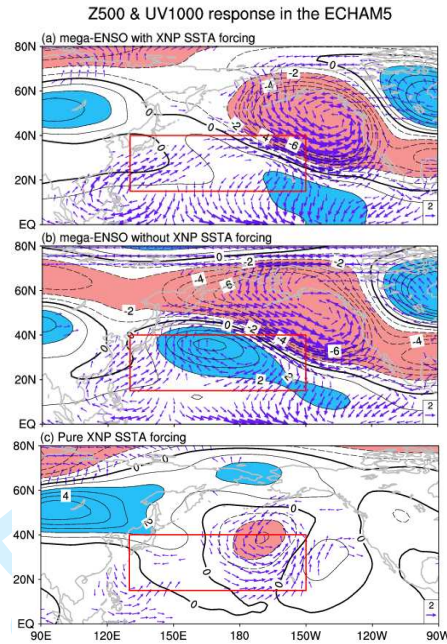
860

861 FIG. 12. The regressions of DJF Z500 anomalies against the mega-ENSO with and

862 without the XNP index signal removed. The shaded areas indicate above 4 hPa or

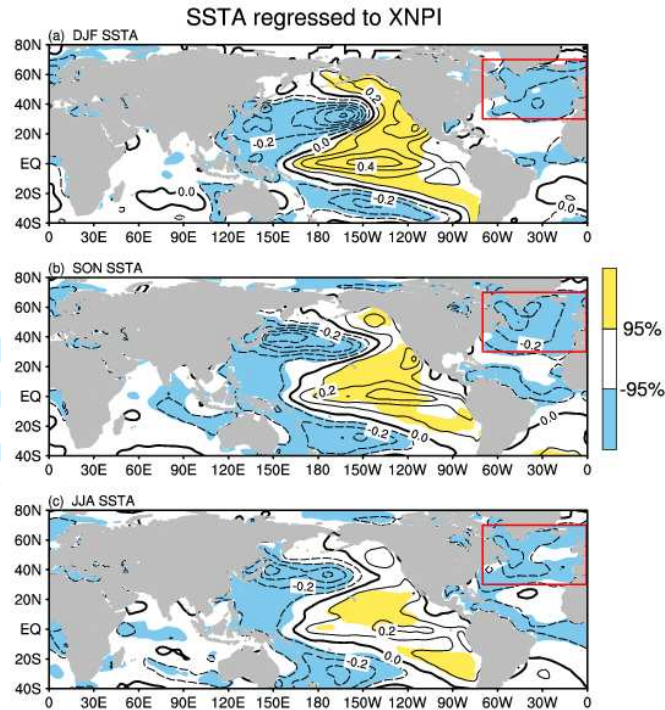
863 below -4 hPa.

864



865
866
867
868
869
870
871
872
873

FIG. 13. (a) DJF Z500 (contours in units of hPa) and UV1000 (vectors in units of m/s) responses in the ECHAM5 regarding a difference between mega-ENSO forcing and control run. (b) Same as (a) but with XNP forcing removed, (c) with pure XNP forcing without mega-ENSO. The shaded areas indicate above 2 hPa or below -2 hPa, wind vectors above 0.8 m/s.



874

875

876

877 FIG. 14. (a) DJF (b) SON and (c) JJA SSTA (contours in units of $^{\circ}\text{C}$) regressed against
 878 the XNP index. The shaded areas exceed 95% confidence level. And the red box
 879 denotes XNA SSTA.

880